Hyper-X Hot Structures Comparison of Thermal Analysis and Flight Data

Ruth M. Amundsen, Charles P. Leonard, and Walter E. Bruce III
National Aeronautics and Space Administration
Langley Research Center
Hampton, Virginia

Fifteenth Annual Thermal and Fluids Analysis Workshop (TFAWS)
August 30 - September 3, 2004 / Pasadena, California

HYPER-X HOT STRUCTURES COMPARISON OF THERMAL ANALYSIS AND FLIGHT DATA

Ruth M. Amundsen, Charles P. Leonard, and Walter E. Bruce III
NASA Langley Research Center
Hampton, VA

ABSTRACT

The Hyper-X (X-43A) program is a flight experiment to demonstrate scramjet performance and operability under controlled powered free-flight conditions at Mach 7 and 10. The Mach 7 flight was successfully completed on March 27, 2004. Thermocouple instrumentation in the hot structures (nose, horizontal tail, and vertical tail) recorded the flight thermal response of these components. Preflight thermal analysis was performed for design and risk assessment purposes. This paper will present a comparison of the preflight thermal analysis and the recorded flight data.

INTRODUCTION

The Hyper-X program is designed to build and test a scaled airframe integrated airbreathing propulsion configuration. Goals of the flight experiment are to demonstrate scramjet performance and operability under controlled powered free-flight conditions at Mach 7 and 10. The Mach 7 flight was successfully completed on March 27, 2004 and the Mach 10 flight is scheduled to fly in the fall of 2004.

The Hyper-X research vehicles are boosted to the required test conditions with a modified Pegasus booster launched from a B-52 carrier aircraft. The flight experiments provide flight data for correlation of ground test data and predictions, experimental techniques and analytical methods for future use in hypersonic vehicle design. Stability and control of the Hyper-X research vehicle is handled by all-moving horizontal tails and vertical rudders that must survive the high aerothermodynamic heating trajectory. The horizontal and vertical tails, along with the vehicle nose are directly in the air stream and undergo substantial heating that can produce large thermal gradients. The purpose of the aeroheating and thermal analysis process was to predict the probable heating loads on the hot structure components and the resultant temperatures. From these temperatures and gradients, a structural analysis could be performed which would demonstrate the deflections and stresses in the material. The temperature predictions are used to verify that all materials remained within their usable temperature ranges.

Thermal analysis of a hypersonic vehicle poses many distinct challenges. The high aeroheating environment demands that the thermal model be robust, and respond well to high loads, abrupt transients and extreme surface fluxes. The material properties must accurately reflect the physical system both in terms of directionality and property variation with temperature, since thermal excursions may be large. The aeroheating environment must be captured accurately, and

variations in flow, time and space must be accounted for. Inherent in this last requirement is that effects of turbulence and shock waves must be represented.

This paper will present thermal flight and analysis results for the Mach 7, Hyper-X, hot structures components. In addition, the basic analysis methodology will be described.

HARDWARE DESCRIPTION

The nose, horizontal tail, and vertical tail on the Hyper-X vehicle are all designed as hot structure components with no active cooling or additional thermal protection such as tiles. High-temperature materials were used in the fabrication of these components to withstand the high temperatures and high thermal stresses. These components are shown in Figure 1 in flight ready configuration on the Hyper-X Mach 7 vehicle.

The nose had a carbon-carbon leading edge and carbon-carbon side chines. The carbon-carbon components were attached to a solid tungsten nose using a tongue and groove design. The carbon-carbon tongue was pinned in the tungsten groove. Only one pin hole was circular for each carbon-carbon component and the other pin holes were slotted to allow for thermal expansion. One thermocouple was installed in the carbon-carbon leading edge at a location 0.5 inch aft of the leading edge flow stagnation point.

The horizontal tail had a carbon-carbon leading edge and a body constructed from Haynes 230 alloy. The carbon-carbon leading edge was attached to the body using the same tongue and groove and pin design as the nose components. The carbon-carbon components were sized to account for thermal expansion so that there would be no forward facing steps during the flight. The Haynes body had pockets milled out of the center section with thin Haynes skin panels welded over the pockets to the ribs to create a smooth and uniform aerodynamic surface. The pockets were milled out of the horizontal body to lighten the tails. Thermocouple instrumentation was installed in the internal pockets with some of the thermocouples attached to the ribs and some attached to the thin skin panels. No thermocouples were installed in the carbon-carbon leading edge.

The vertical tail and rudder were constructed entirely out of Haynes 230 alloy. Similar to the horizontal tail, the vertical tail and rudder had pockets machined out of the body and thin skin panels welded over the remaining ribs to construct lighter weight components. Also, thermocouple instrumentation was installed on the inner pocket ribs and skins.

Thermocouple locations for the hot structure components will be presented in detail in the following sections. Thermocouples used were type K or S, depending on the temperatures expected for that location.

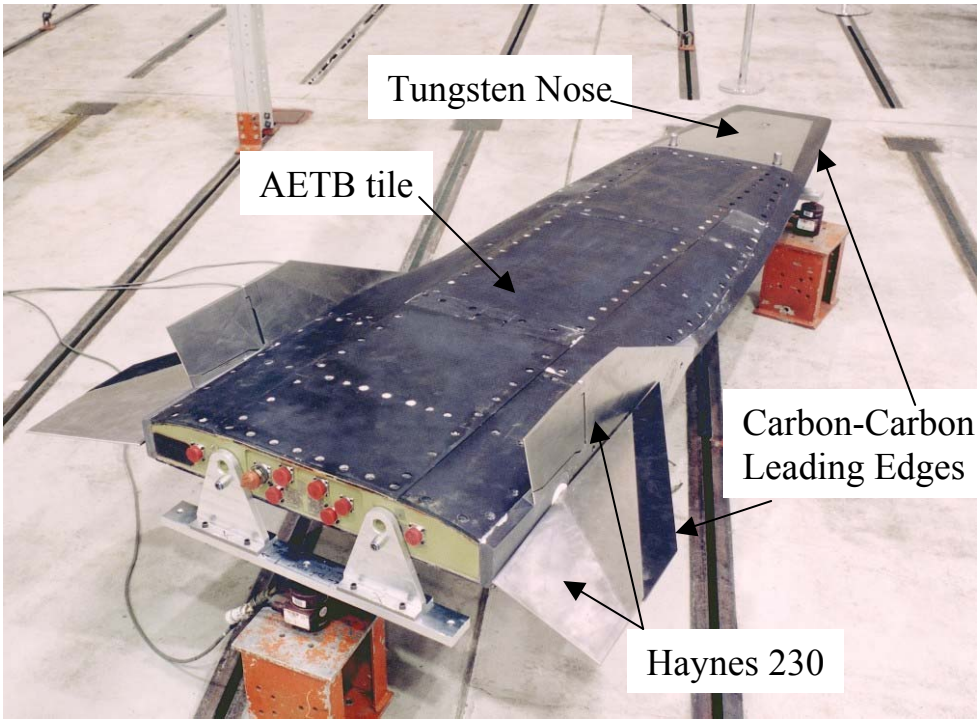

Figure 1. Hyper-X vehicle showing hot structures components.

ANALYSIS METHODOLOGY

The following sections will present the aerothermal and thermal analysis methodology used for making the preflight predictions.

AEROTHERMAL

The Hyper-X Research Vehicle (RV) nose, horizontal tail, and vertical tail are considered hot structure because they do not employ a thermal protection system such as the AETB tile, which covers the majority of the fuselage. The combination of Haynes and carbon-carbon on the control surfaces and tungsten and carbon-carbon on the nose produces a highly three dimensional temperature map. Creation of the temperature field requires an iterative solution between the external convective heat fluxes and the structure's thermal response. Two codes were used to generate the majority of the heat fluxes: StagHeat for the leading edges and SHABP for the acreage.

StagHeat is a code produced specifically for the Hyper-X analysis by Dr Vince Cuda (currently of Swales Aerospace) at NASA Langley. The program is based on Fay Riddell stagnation heating with adjustments for a swept, cylindrical leading edge. StagHeat has been calibrated for real gas and non-continuum effects for the type of trajectories being flown by Hyper-X and for the small 0.030 in leading edge radius through DSMC (Direct Simulation Monte Carlo), VSL (Viscous Shock Layer), and computational fluid dynamics (CFD) codes such as LAURA and GASP. The code was written to easily combine with acreage heating calculations for use in a thermal analysis code.

SHABP (Supersonic Hypersonic Arbitrary Body Program[1]) is a code used widely in government and industry. It employs a suite of impact and shadow methods to solve for the pressure field around hypersonic vehicles. The pressure solution is combined with user selected skin friction routines, which in turn produces heat fluxes. Solutions can be obtained for radiation equilibrium temperature or specified wall temperatures. Wall temperatures can be discrete (different at each node) or uniform. The particular version used (Mark IV) has been modified to produce improved heating results for specified wall temperatures, include NASP derived boundary layer transition criteria, read an external file of flight conditions, and accommodate the GRAM-95 atmosphere.

In addition to the baseline heating results provided by StagHeat and SHABP, additional sources of heating had to be considered, as shown in Figure 2. These augmentations are not calculated directly and must be added externally to the generated heat fluxes. The three phenomena impacting the hot structure design are gap heating, shock interaction from the horizontal tail on the vertical tail, and corner flow at the junctions of the vertical and horizontal tail and the vertical and fuselage. Heat flux multipliers for those three phenomena are derived from literature and are applied to the baseline values by the thermal analyst. The difficulty in application arises from the augmentation varying both temporally and spatially as well as in magnitude depending on the flight condition. Due to the highly configuration dependent nature of the heating augmentation, attempts were made to measure the phenomena during an engine test on a full-scale X-43A in the NASA Langley 8-Foot High Temperature Tunnel for validation purposes. Unfortunately, the data set was not definitive.

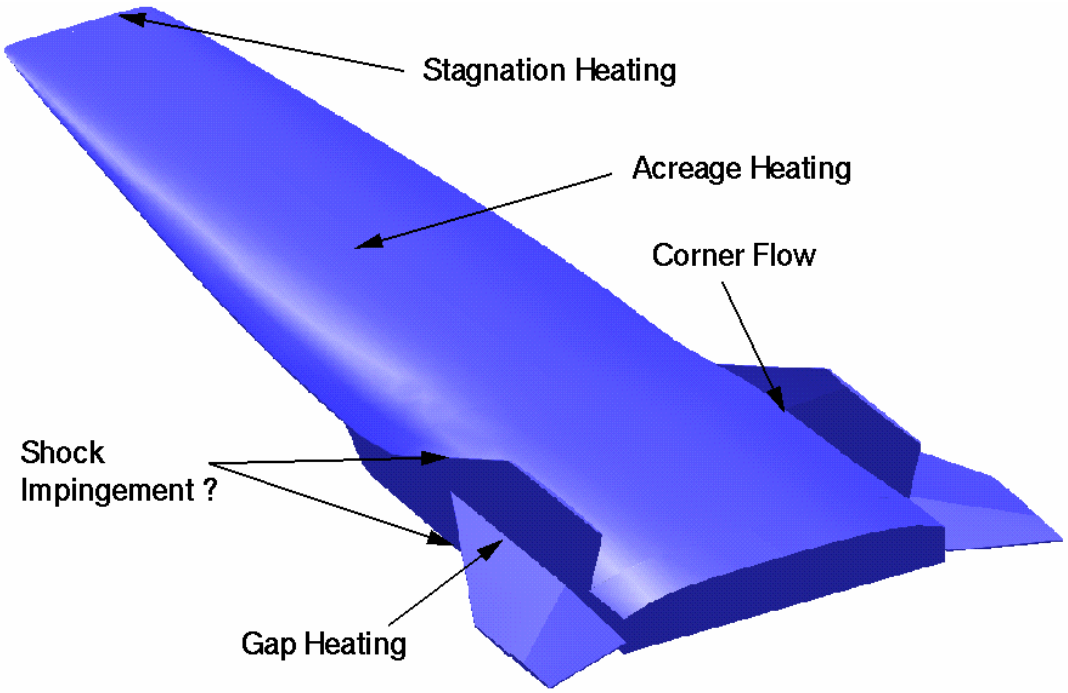

Figure 2. The Research Vehicle experiences heating augmentation from a variety of phenomena.

Engineering codes, such as SHABP and StagHeat, are powerful tools that allow for rapid turnaround, an important asset given the dynamic design environment. Early in the program, multiple designs were considered for the horizontal tail and vertical, varying both materials and architectures. The use of higher order tools was simply time prohibitive. Although the ability to run fully viscous CFD on a full configuration is much more tractable in 2004 than it was at the Hyper-X program's inception in 1996, it is still costly to produce the number of runs required in the conceptual design phase. This is not to say that higher order methods were not used. Although the engineering codes were used to design the hot structure, they were validated by CFD in advance of the analysis against a series of cases enveloping the possible design space and in the final analysis for specific conditions such as maximum heating. Figure 3 shows excellent agreement for a forebody centerline comparison of the CFD tool GASP and SHABP. In addition to comparing engineering codes with a particular CFD tool, multiple CFD codes were also employed throughout the project and were validated against each other. Figure 4 shows LAURA and GASP results for the horizontal tail.

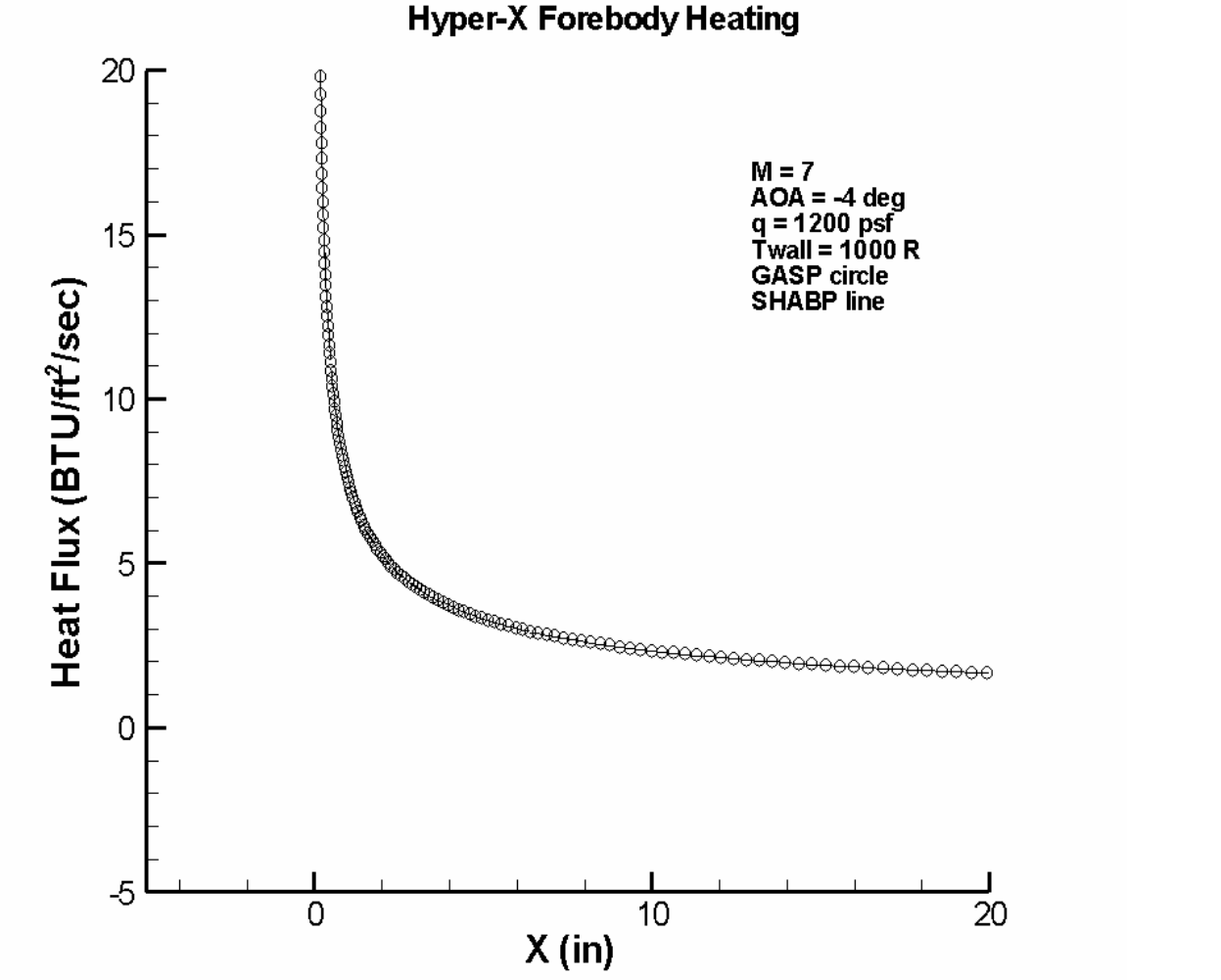

Figure 3. A comparison of forebody heating between GASP and SHABP shows excellent agreement.

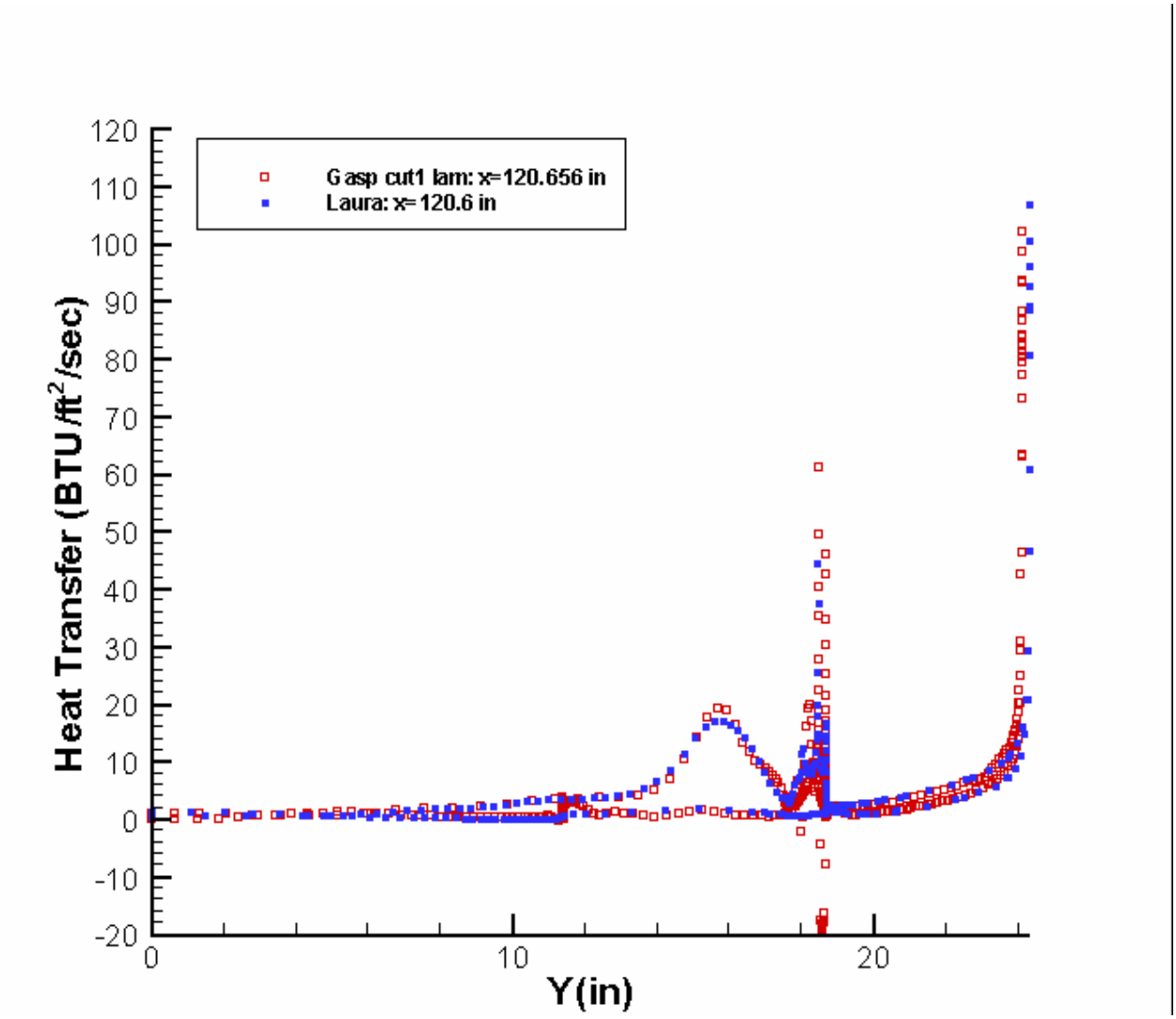

Figure 4. CFD codes are validated against each other for RV horizontal tail.

To produce heat fluxes, the trajectory was discretized for local maxima and minima in the variables that impact heating. Doing so produces a piecewise linear representation of the trajectory. Variables of interest include the Mach number, vehicle angle of attack, dynamic pressure, and control surface deflection. A generic description of the trajectory is shown in Figure 5. Heating was assumed to start at Mach 3 and the heating analyses were performed through closure of the cowl door. While the vehicle continues to fly for several more minutes following cowl door closure, gathering aerodynamic data during its descent into the Pacific Ocean, the hot structure was not analyzed for this portion of the flight as it was beyond the primary success criteria and the vehicle would not be redesigned to survive the post engine test conditions.

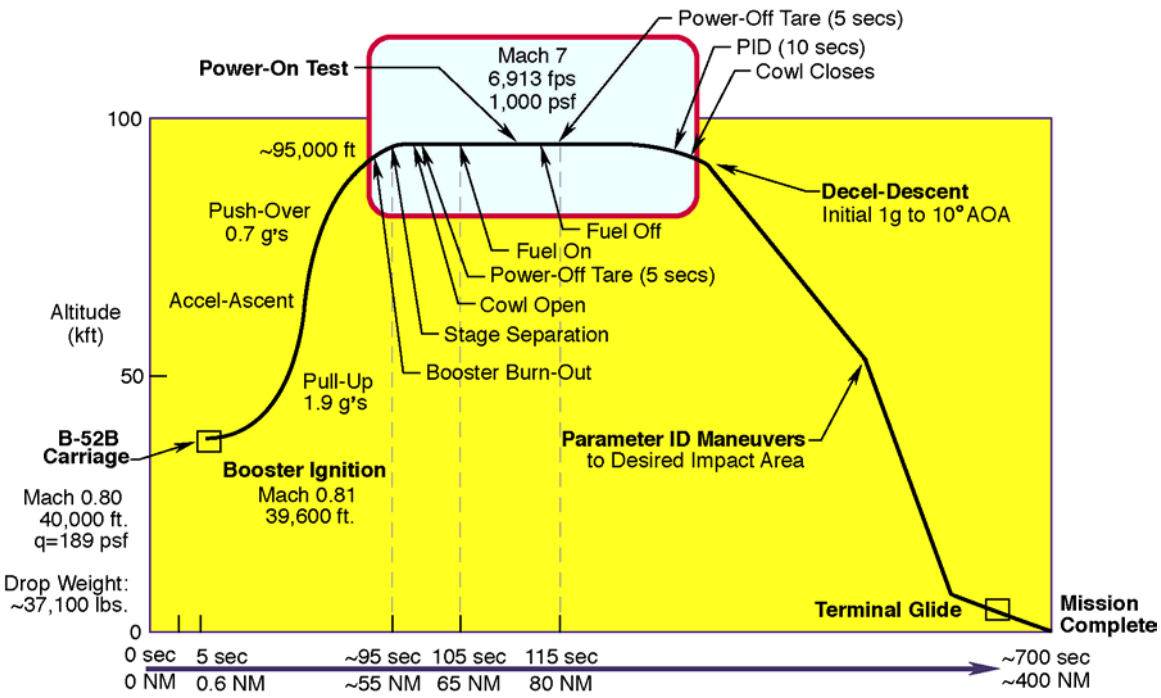

Figure 5. A nominal depiction of the Hyper-X trajectory.

The heat loads produced were associated with an uncertainty based on a root mean squared (rms) combination of the aerothermal code's predictive uncertainty and the trajectory uncertainty. Trajectory uncertainty was ascertained through Monte Carlo analysis. Early in the program, predictive uncertainty was set at 20% based on previous experience with the code. In the actual design process, parametric uncertainties were often used in place of the rms values, particularly if the trajectory was likely to change.

Intrinsic to computing the heat flux to the structure is an assumption or determination of the boundary layer state. Although a momentum thickness Reynolds Number and edge Mach number (Re_θ/M_e) criterion developed in the National Aero-Space Plane (NASP) program existed for determining the state of the boundary layer, turbulent flow was assumed for Mach 7 control surface design purposes. While this decision was thought to be conservative for portions of the horizontal tail based on centerline transition calculations for certain trajectory points, CFD indicated that SHABP even in combination with heating multipliers derived from literature may not be fully representing the complicated flow experienced by the vertical tail. The nose was allowed to transition in the analysis shown below except for the lower surface aft of the boundary layer trips. Turbulent flow was considered to exist immediately downstream of the trip location. Figure 6 shows the comparison between a laminar solution produced using GASP and a turbulent prediction from SHABP for the horizontal tail illustrating the potential conservatism. Preliminary review of flight data (not included here) indicates the transition criterion appears to have accurately predicted the boundary layer state on the centerline of the upper OML showing the upper surface of the RV to be laminar at the later trajectory points. This does not, however, guarantee an accurate prediction for the flow on the control surfaces.

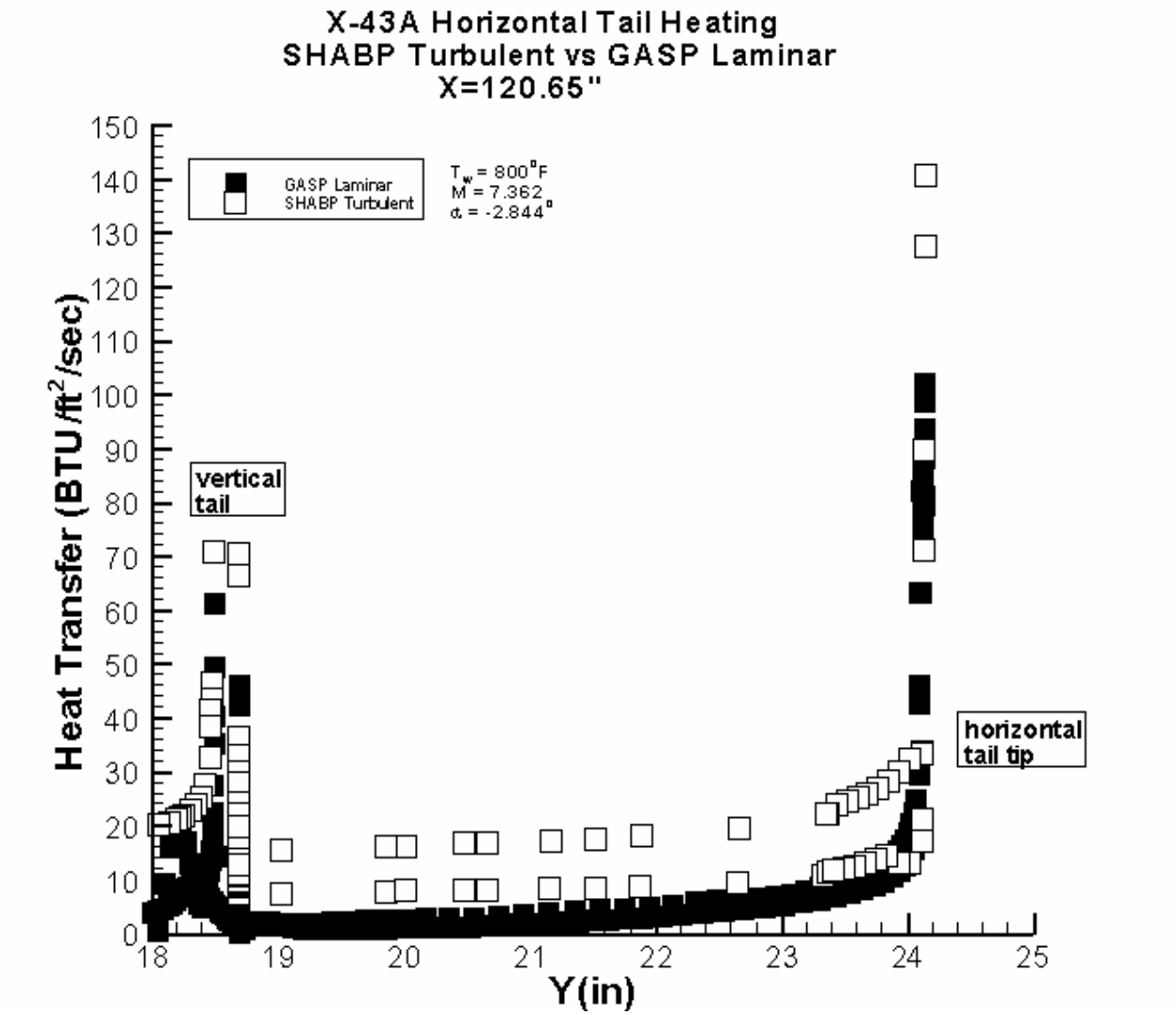

Figure 6. Turbulent heat fluxes predicted by SHABP greatly exceed laminar predictions by GASP.

THERMAL

Thermal modeling was accomplished by importing the geometry from the design program Pro/Engineer, then meshing and performing the analysis in MSC/PATRAN[2]. Several mesh densities were evaluated over the course of the project to ensure that the high heating at the leading edges could be tolerated without leading to numerical instability or smearing of the peak temperature. Mesh at the leading edges was maintained as a hex (brick) mesh, while meshes in other locations with lower heating sometimes utilized a tetragonal mesh. The final mesh on each model is shown in Figure 7 through 9. As an example of mesh density, there were 50,000 nodes and 180,000 elements in the vertical tail model. All material thermophysical properties were functions of temperature. For 3D orthotropic materials such as 5:1 carbon-carbon, material properties were also orthotropic. Radiation to the external variable temperature atmosphere, and radiation within internal cavities, were included.

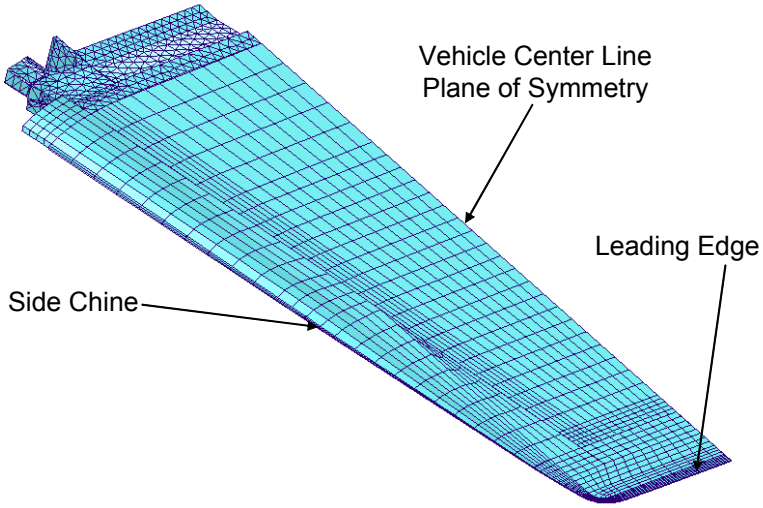

Figure 7. Thermal model mesh for nose.

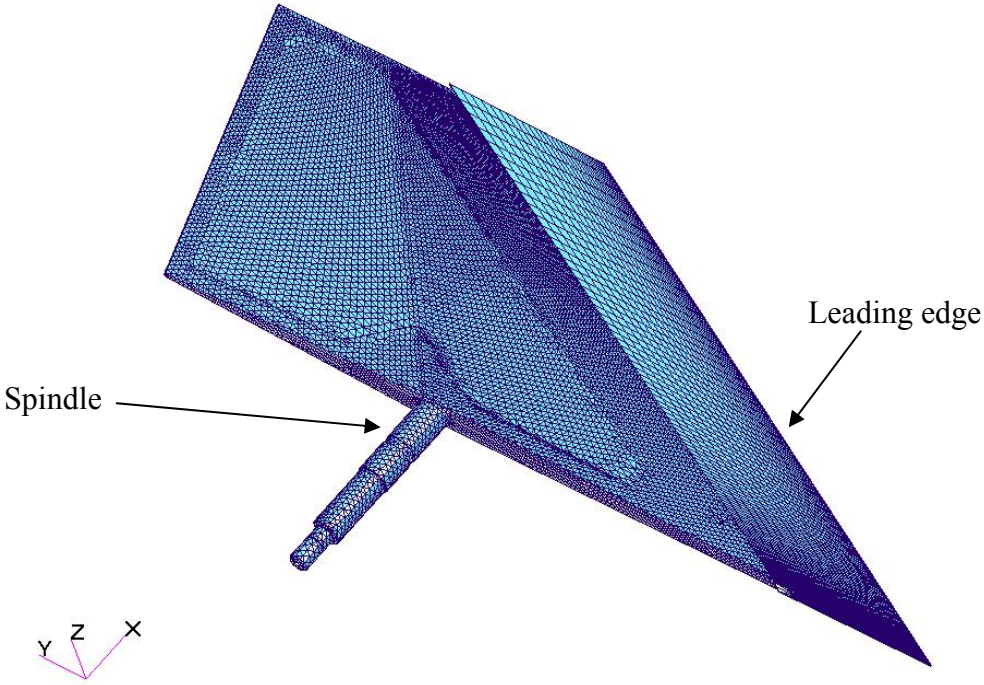

Figure 8. Thermal model mesh for horizontal tail (wing).

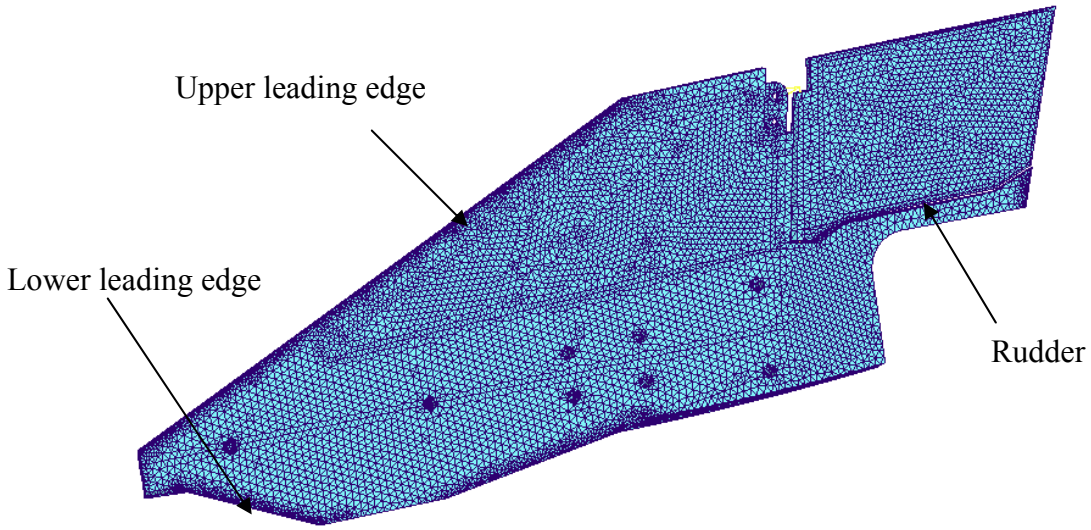

Figure 9. Thermal model mesh for vertical tail.

As previously mentioned, the aeroheating was applied using StagHeat for the stagnation areas and SHAPB for the acreage. Detailed descriptions of these methods can also be found in earlier papers[3,4,5,6,7,8]. Both the stagnation point and SHABP heating loads were only computed at about 20 discrete time steps along the 130-second trajectory, which was a much larger time step than would be used in the thermal analysis. The trajectory began at the time the Hyper-X vehicle was dropped from the B-52. The mesh used in the SHABP model was much coarser than the thermal model would need. Thus, the thermal analysis needed to provide accurate interpolation of the heating data (both in space and time) onto the thermal model. Both StagHeat and SHABP provided maps of heat flux (q) over the specified area at each given time point. These heat fluxes were obviously dependent on the skin temperature of the tail. Thus, after a solution was run for a given set of q maps, the temperature maps were provided back to the aerothermal codes, and new q maps based on the latest temperature prediction were run. Several (3-4) iteration loops were usually required for this cycle to come to closure. Closure was defined as when temperatures between solution sets were varying less than 10°F.

An alternative method was used on the acreage loads for the vertical tail, in order to minimize this iteration time to come to closure. In this method, the SHABP model was run for several uniform wall temperature sets on the entire component, rather than run for a specific predicted temperature gradient. Then, within Patran Thermal, the solver interpolated on temperature as an additional variable, to find the heat load for any given node based not just on the problem time and its location, but also on its temperature at that time. This allowed the problem to be solved in a single run of each program, rather than iterating between them. It also allows for a more detailed map of the skin temperatures to be used to compute the heat flux, and so in regions of sharp thermal gradient, it gives a better representation of the heat flux.

Incorporation of the stagnation loads on the leading edges was fairly straight-forward. Temperatures and body angles for several representative points on each leading edge were used in StagHeat to generate a file of heating versus time for each point. A file in PATRAN format of time-dependent heating based on different body angles along the leading edge was produced. To apply that heating in Patran, a product of functions was used, as shown in equation (1). These determined the difference in temperature between the node the heat is applied to, and the

representative node used to calculate the heating at that body angle, to correct the heating for any given node based on its temperature. What was used in PATRAN is the exact heating for each node based on its temperature, Q_{node}, where

$$Q_{node} = Q_{ref} * \left(\frac{\left(T_{ext} - T_{node}\right)}{\left(T_{ext} - T_{ref}\right)} \right) \quad (1)$$

and where

$$Q_{ref} = h * \left(T_{ext} - T_{ref}\right)$$

Incorporation of the SHABP aeroheating loads was more complex. The SHABP loads were calculated based on the aeroheating grid, a different mesh than the PATRAN model, at 18 time points. These files were pulled into the PATRAN run and interpolated in space and time using user-developed software within a routine provided in PATRAN called ulib. This ulib could include user modifications to subroutines that were called at specific times during the solution. For each node that had an aeroheating boundary condition applied, the thermal solution invoked a umicro.f routine within ulib. This routine determined the nodal position and calculated the aeroheating value via a weighted interpolation of four points in the SHABP grid. Since the SHABP grid was highly swept, and the PATRAN grid was very fine but not regular, being comprised of tetragonal elements, this calculation was not trivial. Due to the high sweep angle in both the SHABP grid and the leading edge itself, and the sharp decrease in aeroheating with distance away from the leading edge, the four points selected might not be the nearest to the node, but needed to bracket it in terms of distance from the leading edge. The interpolation could not be done in the orthogonal x-y axes, but had to be in a system orthogonal to and parallel to the leading edge. This coordinate system was obviously different for the upper and lower leading edges.

An example of the thermal results from the vertical tail is shown in Figure 10. The effect of the high stagnation heating at the leading edge can be clearly seen, as well as the effect of the internal cavities with thin skins heating more than the solid areas.

ANALYSIS COMPARISON WITH FLIGHT DATA

The thermal analysis that was done was intended only to validate this as a robust thermal design, and show whether the vehicle would survive and operate successfully. It was not intended to provide an exact prediction for in-flight temperatures. The engineering tools used for aeroheating will not provide as exact a prediction as a detailed CFD tool. Thus, this analysis was in general conservative. Also, these predictions were based on the trajectory that was predicted to be flown, not on the actual trajectory data taken from the flight. This should also tend to make the analysis conservative.

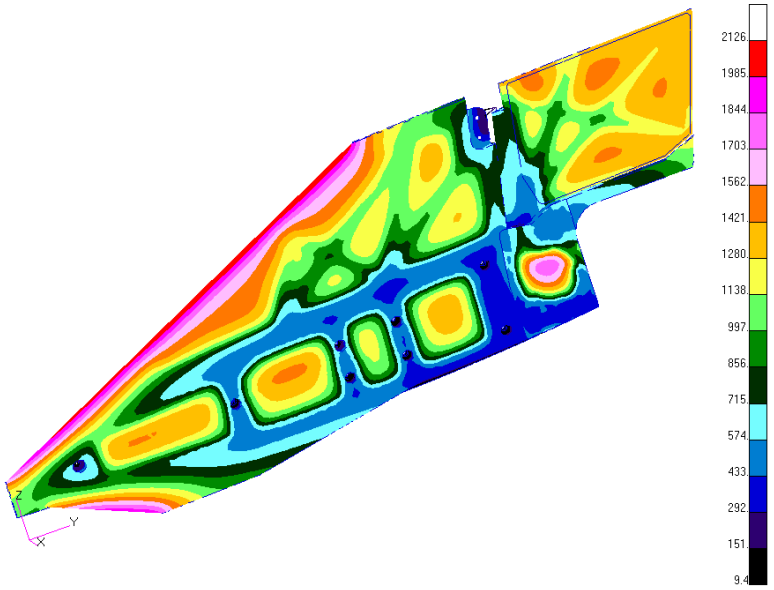

Figure 10. Example temperature distribution at end of trajectory on vertical tail (°F).

NOSE

The nose only had one thermocouple located on a butt line 0.50 inch off the vehicle centerline and at a fuselage station 0.50 inch aft of the leading edge. A comparison of the flight data and the analysis results is shown in Figure 11.

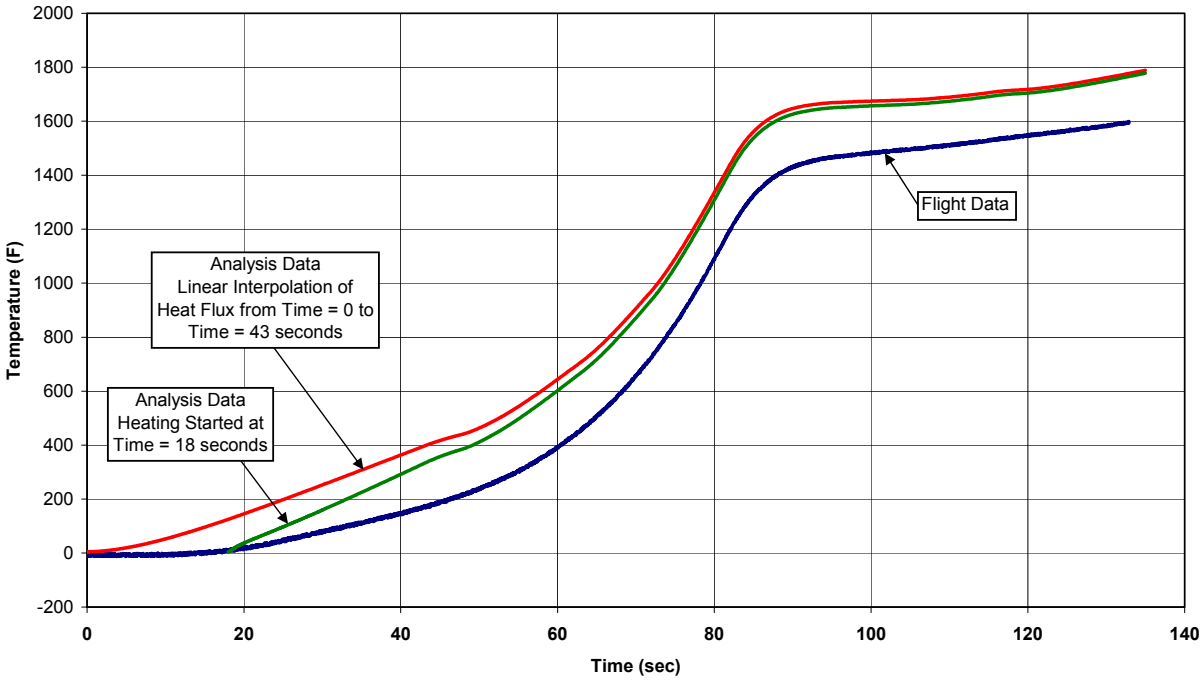

Figure 11. Comparison of nose flight and analysis data.

The analysis is performed by first computing the aerothermal heating rates assuming a spatially varying wall temperature. The aerothermal data is then passed to the thermal code at discrete time points. To reduce the volume of data only 20 discrete time points were used to generate the

aerothermal data. The thermal code then linearly interpolates on the heat flux between these discrete time points and passes the wall temperature profile back to the aerothermal code until closure on the wall temperature is reached.

The thermal analysis was originally performed by linearly interpolating the heat flux data from B52 drop (time = 0.0 sec.) until the first heating data point at approximately 43 seconds. The thermal response using this method is shown in the uppermost curve in Figure 11. Using a linear interpolation for the heat flux from time zero until the first aerothermal heating data point at 43 seconds implied that there was aerothermal heating at transonic and very low supersonic speeds. Since the actual heating during the early part of the trajectory would be negligible, this method was considered to be conservative. The flight data in Figure 11 shows virtually no temperature increase during the first 18 seconds as expected.

The original analysis (upper curve) follows the flight data trend quite well. The temperature magnitude of the analysis is higher than the flight data; this was expected because of the early heating caused by linearly interpolating the heating data between time zero and time 43 seconds. In an effort to improve the correlation the analysis was rerun post-flight with no heating for the first 18 seconds. The heating was then turned on after 18 seconds and the same aerothermal data points were used to rerun the analysis. This second analysis is shown in Figure 11 as the middle curve. It can be seen that the temperature is lower at the earlier time points in the trajectory; however, the temperature quickly climbs towards the original analysis temperature profile with early heating and is virtually the same temperature by 70 seconds into the trajectory. This phenomena has been observed in other analysis where the initial temperature or heating rates in the early parts of the trajectory have little effect on the final temperature. The heating rates are so high and the thermal storage capacity of these thin leading edges are so low that the final temperature and typically the maximum temperature are rather insensitive to the initial temperature or heating rates in the very early part of the trajectory. No additional effort has been made at the time of the writing of this paper to correlate the nose flight data with analysis.

HORIZONTAL TAIL

Ten thermocouples successfully recorded flight data on the horizontal tail. The thermocouple locations and reference numbers are shown in Figure 12. Four of these thermocouples were attached to the inboard, root rib forward of the spindle (T90, T91, T92, and T101), while five thermocouples were attached to the thin skins over the pockets. Three of these skin thermocouples were attached to the lower skins (T102, T108, and T110) and two were attached to the upper skins (T109 and T111). Of the two upper skin thermocouples one was on the left horizontal (T109) and one was on the right horizontal (T111) at approximate symmetric locations. An additional thermocouple was attached to the spindle shaft (T62). Unfortunately, thermocouples T64 and T89 were inoperable prior to flight and could not be repaired; therefore, no flight data exist for these thermocouples. No thermocouples were installed in the carbon-carbon leading edge.

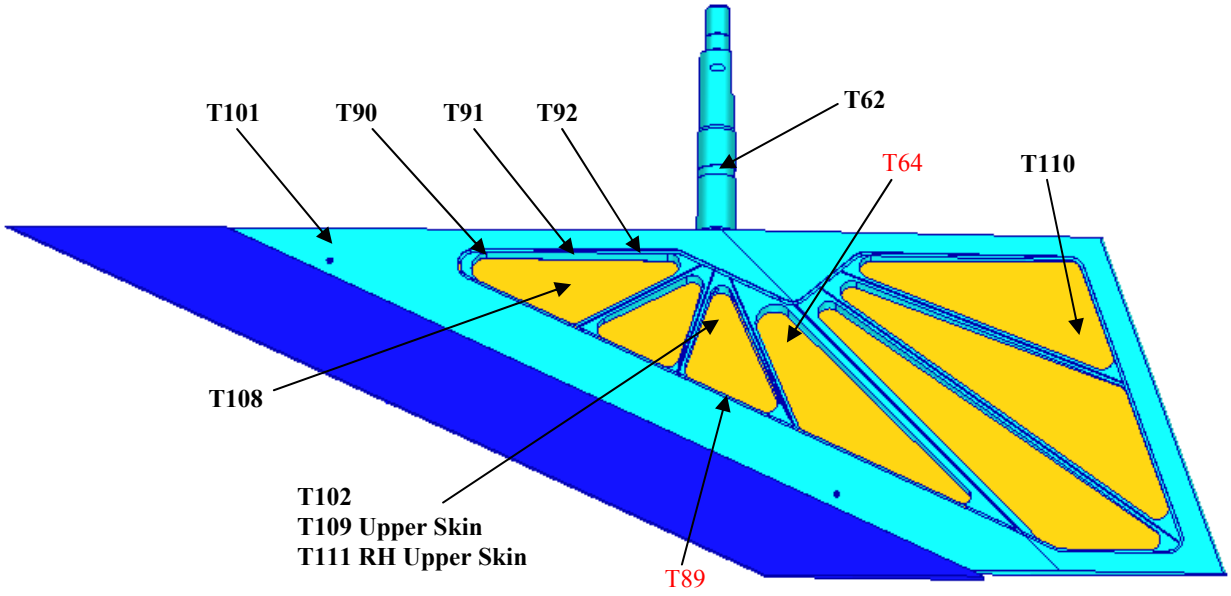

Figure 12. Left hand horizontal instrumentation locations (upper skin removed).

The flight and analysis data from the four root rib thermocouples had very similar trends and profiles; only the magnitude of the temperatures were substantially different. A comparison of the flight thermal data and the analysis data is shown for thermocouple 101 in Figure 13.

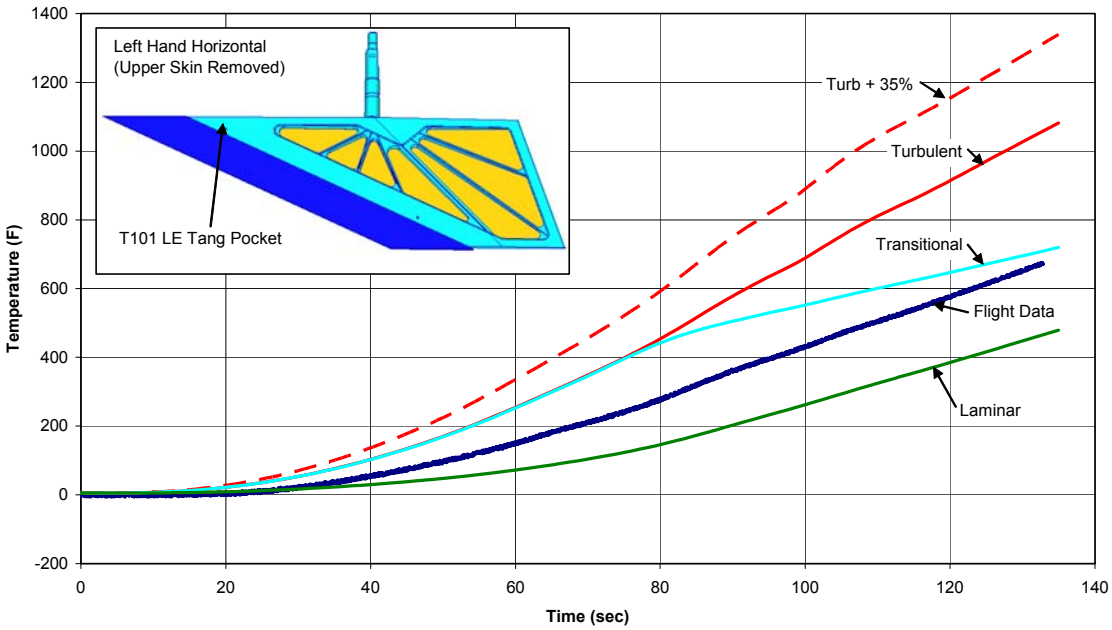

Figure 13. Comparison of flight and analysis data for thermocouple 101

The flight data for thermocouple 101, presented in Figure 13, shows that there is little or no thermal response at this location until approximately 18 seconds into the flight. The temperature then increases until about 60 seconds at which point the temperature increase maintains a

relatively constant slope until the end of the engine test at 134 seconds. As mentioned above, the other three root rib thermocouples also exhibit the same characteristic.

In addition to the flight data, four sets of analysis data are also presented in Figure 13. The original design concept for the horizontal tail was to generate a solution assuming a fully turbulent boundary layer for the entire trajectory. In addition, to account for trajectory uncertainties, method uncertainties, and the potential of trajectory changes after analysis completion, a factor of 35% was applied to the heat flux which is shown in Figure 13 as the uppermost curve. This was considered to be a conservative design approach because of the uncertainty of the boundary layer state associated with the complex flow-field over the horizontal tail. Also, there is the issue of the gap heating on the inboard root of the horizontal. This was accommodated by applying additional heating factors to the gap heating region.

To assess the magnitude change in temperature that would be associated with a boundary layer change two additional solutions were generated. The aerothermal heating was computed assuming a laminar boundary and a transitional boundary layer. These solutions are also presented in Figure 13. The transitional solution assumes the boundary layer changes from turbulent to laminar when a specific flow-field criteria is met. From observation the transitional solution follows the turbulent solution until almost 80 seconds at which point the temperatures start to diverge from the turbulent solution and start to approach the laminar solution.

The flight data appears to fall between the turbulent and the laminar solution and exhibits the same general characteristics of these two solutions with a continuous temperature increase. The slope of the temperature increase from 80 seconds until the end of the analysis is relatively constant for the turbulent and laminar analysis, and the flight data. The transitional solution does not exhibit the same general characteristic as the flight data, exhibiting a slope change in the temperature increase at approximately 80 seconds.

Flight and analysis data are presented for three additional thermocouples (thermocouples 102, 109, and 111) which are shown in Figure 14 and Figure 15. Thermocouples 102 and 109 are at the same fuselage station and butt line on the left horizontal with thermocouple 102 being attached to the lower panel and thermocouple 109 being attached to the upper panel. Thermocouple 111 is in an identical location to thermocouple 109 on the right horizontal upper panel.

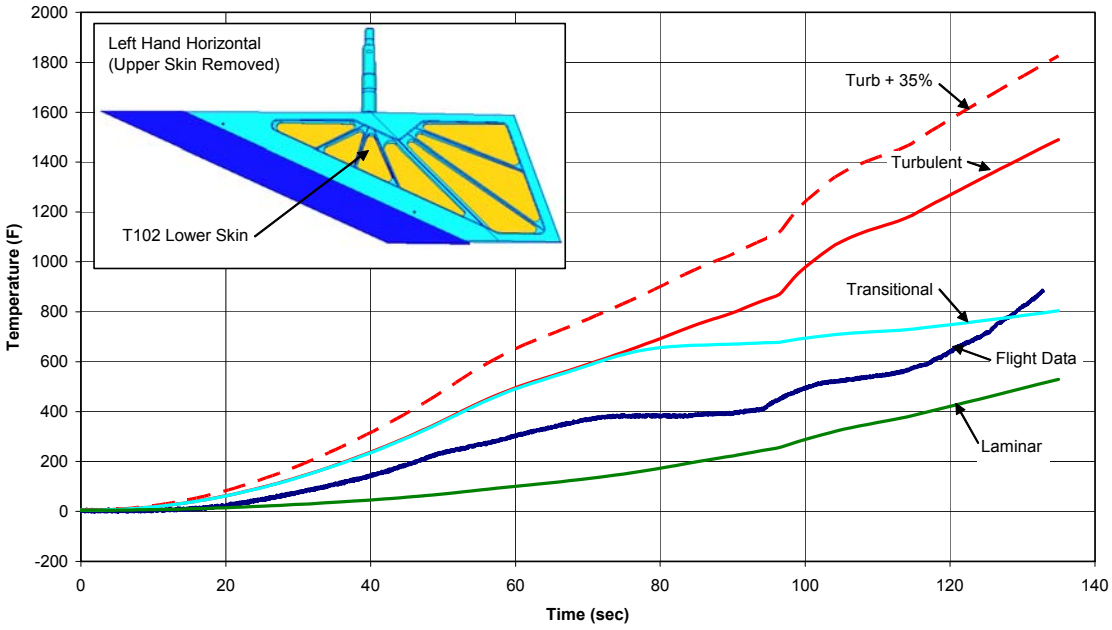

Figure 14. Comparison of flight and analysis data for thermocouple 102.

The flight data for thermocouple 102, presented in Figure 14, shows that the temperature gradually increases until approximately 70 seconds. At 70 seconds the temperature starts to level off until approximately 95 seconds when the temperature slope dramatically increases. At around 60 seconds the booster and the Hyper-X vehicle start to push over as they approach flight altitude. At this point in the trajectory the horizontal tail changes from a positive angle of attack to a negative angle of attack meaning the lower panel, where thermocouple 102 is attached, goes from the windward side to leeward side. When the lower panel is on the leeward side the heating rate reduces resulting in a slope change in the temperature profile. At approximately 95 seconds the Hyper-X vehicle separates from the Pegasus booster. When separation occurs the horizontal tail abruptly changes to a positive angle of attack resulting in increased heating to the lower panel. The sudden increase in heating at separation results in a rather abrupt increase in temperature at approximately 95 seconds which is seen in the flight data. After separation the wing angle of attack slowly decreases, but still stays positive, until approximately 112 seconds, when the angle of attack starts to increase again. From inspection of the thermal flight data it appears that the response of thermocouple 102 follows the wing angle of attack profile. The thermal profile for the other two thermocouples attached to the lower skin (thermocouples 108 and 110) also exhibit a very similar thermal profile.

Four analysis thermal solutions are also presented in Figure 14. They are a fully turbulent boundary layer solution, laminar solution, transitional boundary layer solution, and the design condition of the turbulent solution with a 35 percent factor added to the heat flux. The turbulent solution, even though at a higher overall magnitude, captured the separation temperature increase. There is also a temperature slope change for the laminar and transitional solutions at separation, except it is very subtle and not well pronounced. As with the root rib thermocouples, the flight data falls between the turbulent and laminar analysis solutions. Therefore, it would be natural to assume that the transitional solution would more closely match the flight data as the boundary layer would be expected to transition from turbulent to laminar during the course of

the flight. However, inspection of the data shows that the transitional solution does not exhibit the correct characteristic and does not accurately capture the heating increase toward the end of the flight. This indicates that the flow field is potentially more complex than has been modeled and all of the physics of the flow may not have been captured in the modeling efforts. Additional efforts to correlate the flight data have not been completed as of the writing of this paper.

Only one thermocouple was located on the right hand horizontal (thermocouple 111) and it was positioned to match the location of a thermocouple on the left horizontal (thermocouple 109). Both thermocouples were attached to the upper skin panel and are at the same fuselage station and absolute butt line value referenced to the vehicle centerline as thermocouple 102 which was attached to the lower skin. This presented a unique set of matched data between the left and right horizontal and the upper and lower skin. The data for thermocouples 109 and 111 are presented together in Figure 15.

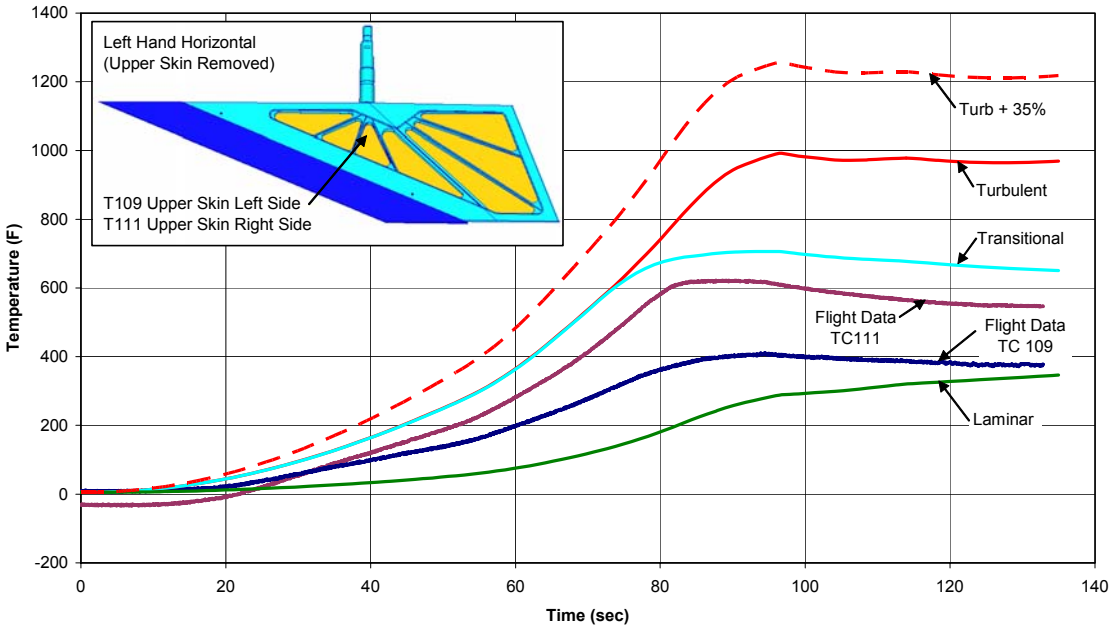

Figure 15. Comparison of flight and analysis data for thermocouples 109 and 111.

Inspection of the flight data in Figure 15 shows that the results on the right and left horizontal are not the same. The expectation was that the left and right temperature profiles for these two thermocouples would be virtually identical since there was no indication in the flight data of different angles of attack for the two horizontals or any other flight variables that would indicate a difference in the flow over the horizontals. Unfortunately, there are no other thermocouples on the upper skins of either horizontal which can be used for comparison.

It can be noticed that at the time of separation (approximately 95 seconds) thermocouple 102 and thermocouple 109, both on the left horizontal on the lower skin and upper skin respectively, are reading the same temperature of approximately 400 ºF. At the same time the thermocouple on the upper right horizontal skin is reading about 220 ºF hotter. Another difference between the two matched thermocouples is the initial temperature. The initial temperature of all of the left horizontal thermocouples was approximately 5 ºF while the initial temperature of the right hand

horizontal thermocouple was approximately -31 ºF. The B-52 carrier aircraft recorded an outside, ambient air temperature of -40 ºF at drop altitude. It is important to note that the instrumentation was selected and ranged to have high accuracy at the expected flight temperatures. Therefore, it is possible that the thermal measurements at the relatively low initial temperature may not be extremely accurate. One more important item is that the thermal gradients on the thin skin panes are very high in certain locations; therefore, the absolute temperature is very sensitive to location. If the thermocouple flight location or analysis node location are not well matched this could also produce an unintended temperature difference. At the time of the writing of this paper this difference between the left and right thermocouple readings had not been resolved, and will be investigated further

The corresponding analytical results are also plotted in Figure 15 with the flight data. As with the previous sets of data, the flight data for thermocouples 109 and 111 fall between the laminar and transitional analysis data. The analysis data does not help resolve the difference between the right and left temperature differences and will be an item of future analysis.

VERTICAL TAIL

Predictions for the vertical tail thermocouples (TCs) were generated by selecting the closest nodes within the thermal model to each thermocouple point, and plotting the temperatures of those nodes. This method does not include the detail of the mass of each thermocouple and its attachment to the vehicle structure, but with the high temperatures experienced by these components, that loss of rigor should be inconsequential. The thermocouple locations for the vertical tail are shown in Figure 16. On the outboard faces of both the tail body and rudder, there was a skin of material, 0.090" (2.3 mm) thick, covering the pockets where the thermocouples were placed; that skin is removed here for showing the internal geometry of the tail. TCs that were not operational during flight were T086, T096 and T112. Unfortunately, these latter two were of great interest as the farthest forward of the TCs installed on a thin skin area. The sole remaining TC that has a similar short distance to the leading edge is T093.

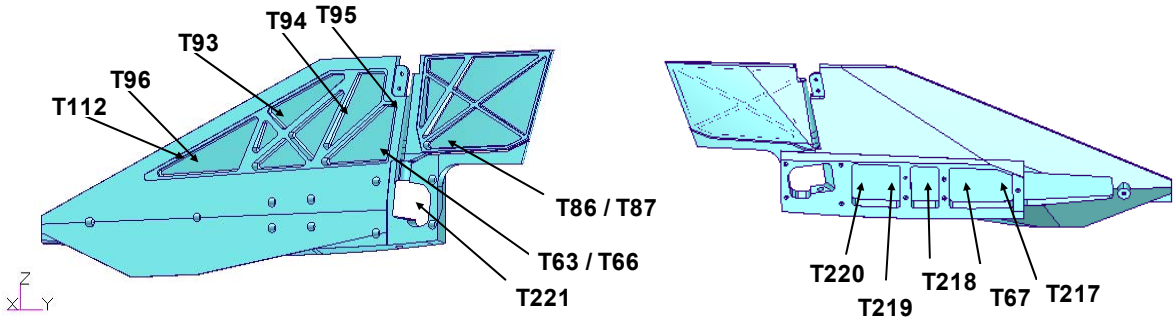

(a) outboard view **(b) inboard view**

Figure 16. Thermocouple locations on vertical tail.

In general, the predictions made before flight fairly well bounded the flight data or were conservative; i.e. the flight data curve was between the nominal prediction and the +35% margin prediction, or fell below the nominal prediction. This was expected since the analysis was designed to be conservative. Several of these plots are shown below. Figure 17 is representative of the TCs within the gap area, on the rudder, or enclosed in a solid block of material; this

included eight of the TCs. These predictions were conservative, and the prediction showed the same trend as the flight data. Figure 18 shows the response of the two TCs on a skin area well aft on the tail (T063 and T066); for these, the nominal and 35% margin runs bracketed the flight data. The heating is obviously somewhat higher than was predicted for the nominal case. One item of interest on this plot is that these TCs, placed symmetrically on the left and right vertical tails, exhibit well-matched behavior. This an indication that there is no unexpected yaw or side-slip that would lead to increased heating on one side. Farther forward on the tail, Figure 19 shows the response of the only two TCs that were operational on a thin skin area on the forward portion of the tail, T093 and T094. On these TCs, the heating was much higher than predicted, and the flight data actually breaks above the 35% margin case at about 83 sec.

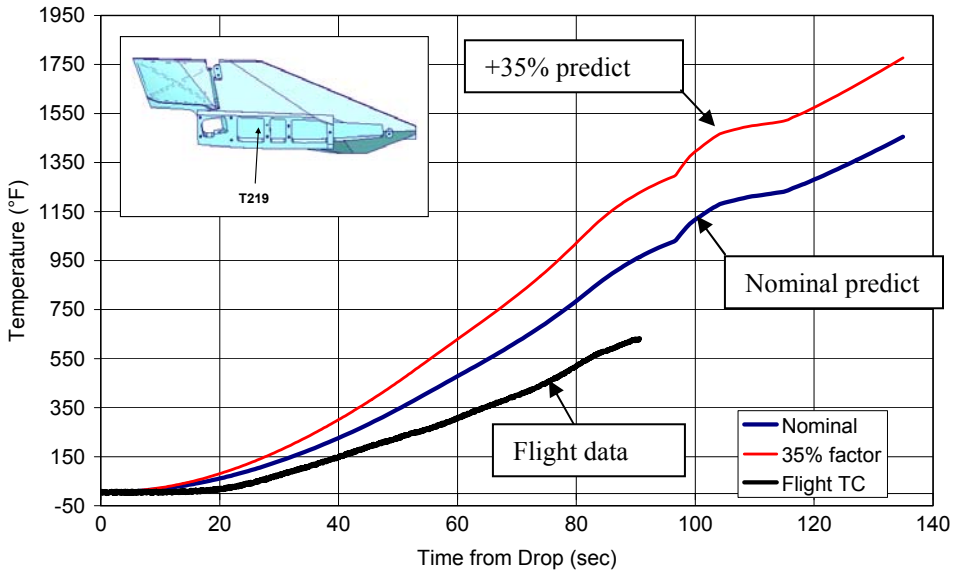

Figure 17. Flight data compared to prediction for T218.

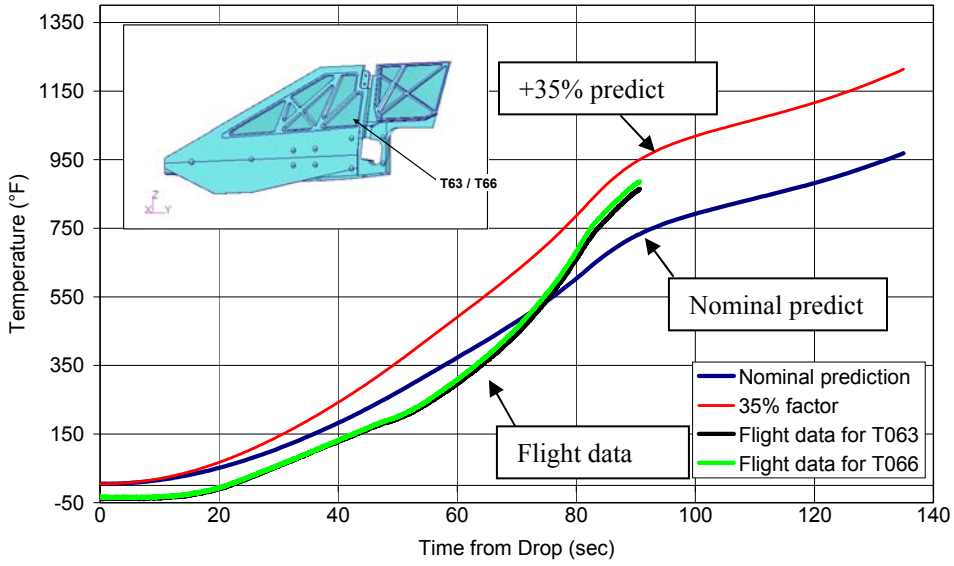

Figure 18. Flight data compared to prediction for T063/066.

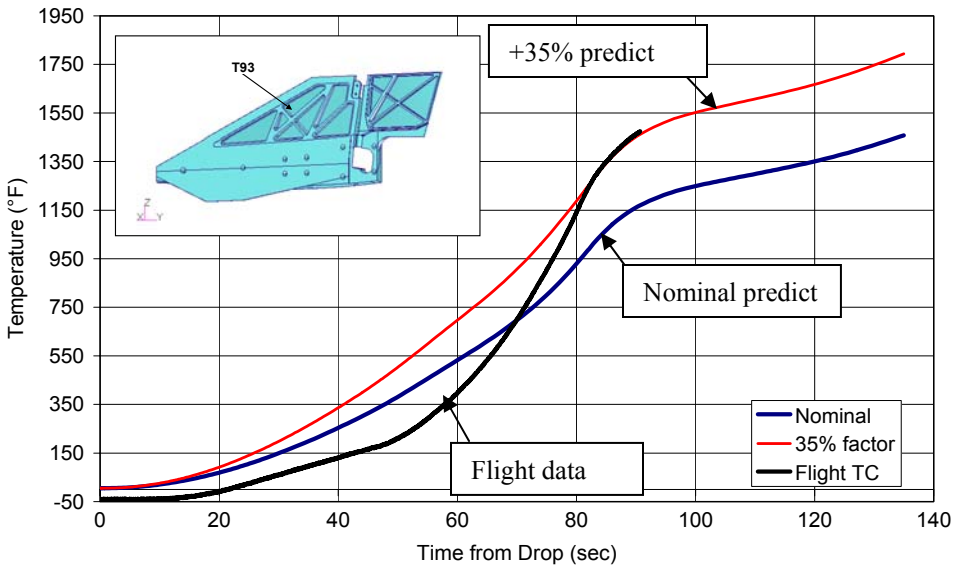

Figure 19. Flight data compared to prediction for T093.

One obvious feature of these curves is that the initial steady state condition assumed at the drop (0 seconds), was incorrect. The actual temperature of most of the TCs at drop was about -40°F, as compared to the conservative assumption made before flight, that they might be as warm as 5°F. This correction was made for subsequent runs.

In order to help understand differences between the flight data and the thermal predictions, one interesting feature to examine is the rate of change of temperature, or the slope of the curve. For both T093 and T094, the slope curve shows a huge change in the behavior at about 46 seconds after drop, as shown in Figure 20. The other TCs, such as those in the gap area, do not show anything like this abrupt change in slope; their slope increases smoothly. Figure 20 also shows that this behavior for T093 is not seen in the initial predictions. There is a slight inflection of the slop curve near 50 seconds, but nothing like the abrupt change seen in the flight data.

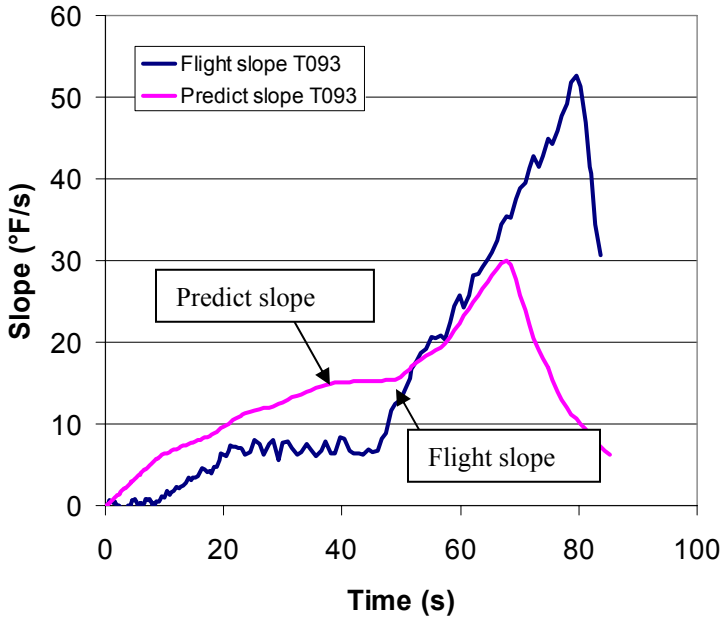

Figure 20. Slope of T093, flight data versus initial prediction.

Several changes in the model were attempted in order to duplicate this sharp change in slope at 46 seconds, and come closer to the flight data. One change was to go to the alternate method of applying heat loads, where the heat loads are predicted for a set of uniform wall temperatures, and the Patran Thermal solver interpolates to find the heat load for a node based on its temperature. Using this method, the slope and temperature curve comparison is shown in Figure 21. The slope mimics the flight data better, and shows a slight inflection at 46 seconds, but does not have as radical a change in slope as the flight data. In this case the +35% margin case is lower, because with the skin temperature rise taken into account, the 35% margin does not have as direct an effect.

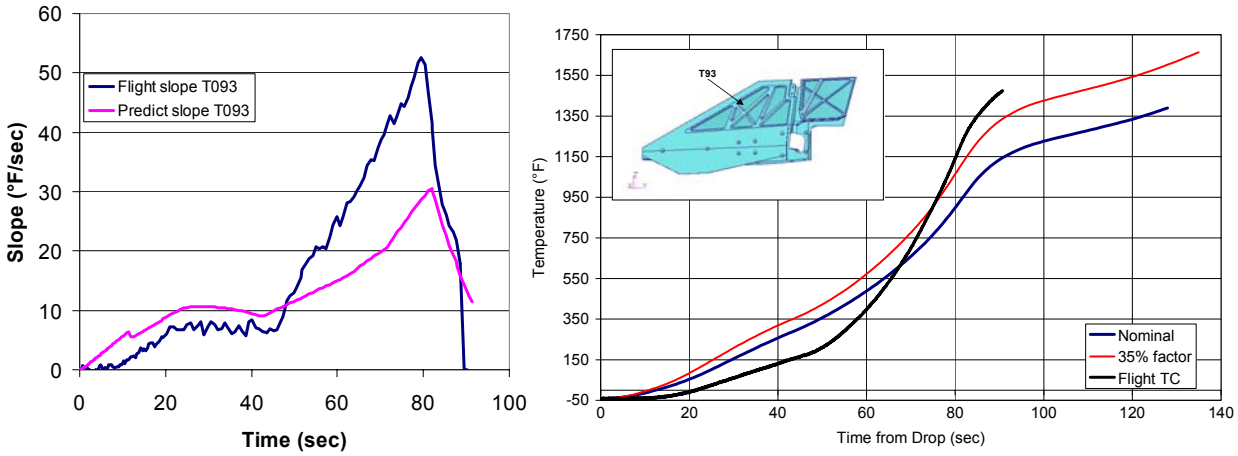

(a) slope comparison **(b) temperature comparison**

Figure 21. Slope and temperature prediction using uniform wall temperature method.

Because most of the thermocouples are predicted with conservatism, it cannot be an error in material properties, optical properties or contact boundary conditions that is causing the under prediction of T093 and T094. Because these TCs are the closest to the leading edge, it was thought that the stagnation heating might be underpredicted, and that an increase in stagnation heating could bring the prediction in line. Artificial increases of several different values in the stagnation heating were used, with no effect on these TCs. The heating that is applied in the model from time 0 seconds up to the first trajectory time step of 42.8 seconds uses a simple linear growth from zero heating to the value at 42.8 seconds. Since this increase will in fact probably not be linear, one change that was tried was to have the heating increase in parabolic manner. This was not successful in improving the match with the flight slope. Other changes evaluated were to have the internal solver evaluate at the beginning or end of each time step, rather than in the middle of the time step, as was the default method. This change did not alter the predictions appreciably.

The TCs with too-low predictions are seen on the forward part of the outboard skin, and the major split between flight data and prediction occurs when near the first time point in the trajectory, when the shock augmentation factors on the tail begin. Thus, it was hypothesized that there was some flow pattern that was not being captured, leading to an increase in heating on the skin in that location. In order to try and simulate that, the shock angle on the upper surface of the vertical was artificially increased by a factor of up to 6, and the magnification of augmentation was increased by a factor of 3. Even this artificial boosting of the shock augmentation did not begin to simulate what is actually occurring in flight. (One reason these were not very effective was that the first time point at which a shock wave that can be

augmented occurs on the upper part of the tail is at 63 seconds, well past the region at which a change must initiate.) This behavior is something to be evaluated further in future work.

CONCLUSIONS AND FUTURE WORK

In general, current methods have yielded reasonable predictions of the flight behavior for Hyper-X at Mach 7, with most predictions being conservative. The actual flight trajectory data (actual Mach number, altitude, etc. versus time) were only recently available, so more will be done using that data to improve the modeling and the accuracy of the correlation. The differences in behavior for the left and right horizontal tail will be further investigated. For the anomalous behavior on the forward portion of the vertical tail skins, it may be that in order to achieve a realistic prediction, a more rigorous aerothermal model will need to be used, such as a CFD model. Also, potential shocks on the upper surface early in the trajectory will be evaluated.

ACKNOWLEDGEMENTS

The authors would like to acknowledge the support of the Hyper-X project, as well as the work of Michael Lindell in structural modeling, Robert Dillman in geometry generation, Mark Anderson in aeroheating translation code development, and Dr. Vince Cuda in heating code development. Thanks are also due to Tom Jentink and Glenn Bobskill for use of their GASP solutions, and to William Wood for his LAURA solutions.

CONTACTS

Ruth M. Amundsen, Ruth.M.Amundsen@nasa.gov

Charles P. Leonard, Charles.P.Leonard@nasa.gov

Walter E. Bruce III, Walter.E.Bruce@nasa.gov

NOMENCLATURE, ACRONYMS, ABBREVIATIONS

AOA	Angle of Attack
CFD	Computational Fluid Dynamics
DSMC	Direct Simulation Monte Carlo
GASP	General Aerodynamic Simulation Program
LAURA	Langley Aerothermodynamic Upwind Relaxation Algorithm
NASP	National Aero-Space Plane
OML	Outer Mold Line
rms	root mean squared
SHABP	Supersonic Hypersonic Arbitrary Body Program

TC	Thermocouple
VSL	Viscous Shock Layer

REFERENCES

[1] Gentry, A.E.; Smith, G.N.; Wayne, Oliver: The Mark IV Supersonic Arbitrary Body Program, AFFDL-TR-73-159, Volumes I, II & III, November 1973.

[2] MSC/PATRAN User Manual, MacNeal-Schwendler Corporation, Version 2000 (r2), August 2000.

[3] Amundsen, Ruth M.: "Method Improvements in Thermal Analysis of Mach 10 Leading Edges," presented at the Tenth Conference, Workshop and Product Presentation on Thermal and Fluids Analysis Tools and Methods, NASA Huntsville, AL September 13-16, 1999.

[4] Amundsen, Ruth M.: Comparison of Integrated Analysis Methods for Two Model Scenarios, Ninth Conference, Workshop and Product Presentation on Thermal and Fluids Analysis Tools and Methods, Cleveland, Ohio, August 31--September 4, 1998.

[5] Amundsen, Ruth M.; and Leonard, Charles P.: "Hypersonic Thermal Analysis including Shock Interaction Load Amplification with Motion Effects", 27th Annual Conference on Composites, Materials and Structure, January 27-31, 2003, Cocoa Beach, Florida.

[6] Lindell Michael C.; and Amundsen, Ruth M.: "Nonlinear Thermal/Structural Analysis of Hypersonic Vehicle Hot Structures", presented at the NASA Workshop on Innovative Finite Element Solutions to Challenging Problems, NASA GSFC, May 2000.

[7] Amundsen R.M.; and Torres, A. O.: "Thermal Analysis of the Hyper-X Research Vehicle Wing: Mach 7 Design," presented at the 97 JANNAF Conference, Chemical Propulsion Information Agency, West Palm Beach, Florida, October 27-31 1997.

[8] Amundsen Ruth M.; and Brzowski, Matt: "Correlation of Thermal Model with Hyper-X Leading Edge Material Testing," presented at the 25th Annual Conference on Composites, Materials and Structures, Cocoa Beach, Florida, January 22-26, 2001.